

Review of mathematics, numerical factors, and corrections for dark matter experiments based on elastic nuclear recoil

J.D. Lewin ^{*}, P.F. Smith

Particle Physics Department, Rutherford Appleton Laboratory, Chilton, Didcot, Oxon, OX11 0QX, UK

Received 10 April 1996; revised 31 May 1996; accepted 8 June 1996

Abstract

We present a systematic derivation and discussion of the practical formulae needed to design and interpret direct searches for nuclear recoil events caused by hypothetical weakly interacting dark matter particles. Modifications to the differential energy spectrum arise from the Earth's motion, recoil detection efficiency, instrumental resolution and threshold, multiple target elements, spin-dependent and coherent factors, and nuclear form factor. We discuss the normalization and presentation of results to allow comparison between different target elements and with theoretical predictions. Equations relating to future directional detectors are also included.

1. Introduction

A number of experiments are underway or planned to investigate the hypothesis that the unidentified non-luminous component of our Galaxy might consist of new heavy weakly interacting particles. The experiments aim to detect, or set limits on, nuclear recoils arising from collisions between the new heavy particles and target nuclei.

The majority of experiments are based on ionization, scintillation, low temperature phonon techniques, or some combination of these. They have in common the same basic theoretical interpretation. The differential energy spectrum of such nuclear recoils is expected to be featureless and smoothly decreasing, with (for the simplest case of a detector stationary in the Galaxy) the typical form:

$$\frac{dR}{dE_R} = \frac{R_0}{E_0 r} e^{-E_R/E_0 r} \quad (1.1)$$

where E_R is the recoil energy, E_0 is the most probable incident kinetic energy of a dark matter particle of mass M_D , r is a kinematic factor $4M_D M_T / (M_D + M_T)^2$ for a target nucleus of mass M_T , R is the event rate per unit mass, and R_0 the total event rate. Since Galactic velocities are of order $10^{-3}c$, values of M_D in the 10–1000 $\text{GeV}c^{-2}$ range would give typical recoil energies in the range 1–100 keV.

^{*} Corresponding author. E-mail: j.d.lewin@rl.ac.uk.

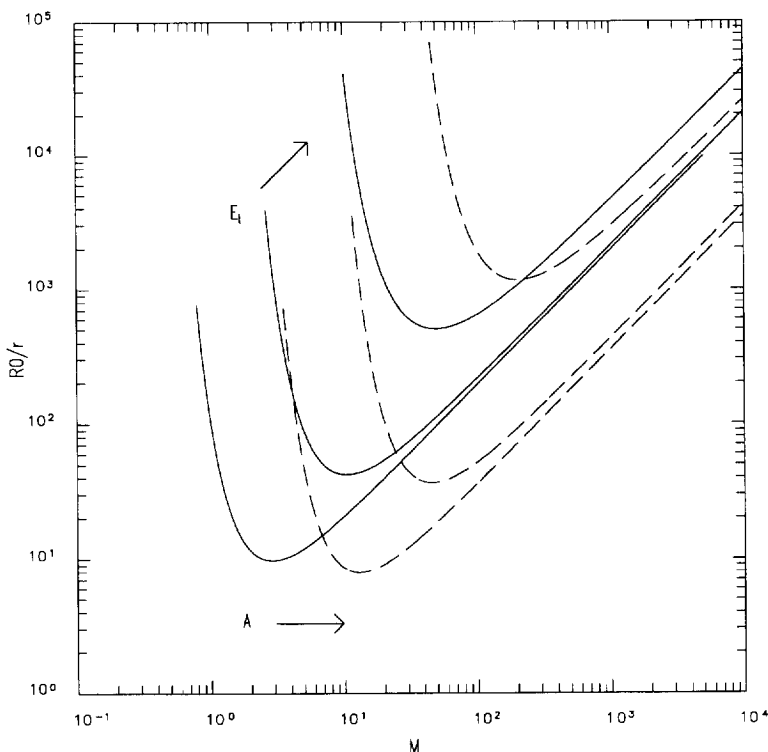


Fig. 1. Typical shape of limit curves; — small A , - - - large A , each for three values of E_1 increasing from left to right.

All the experimental efforts lie on the left-hand side of (1.1)—the aim being to progressively reduce or reject background events to allow a spectrum of rare nuclear recoil events to be observed. In particular, underground operation is preferred, to eliminate nuclear recoils from neutrons produced by cosmic ray muons; and methods of discriminating between nuclear and electron recoils are being developed, to reject gamma and beta-decay background in the target and detector components.

When an experiment has set an upper limit to the differential rate at any particular value of E_R , the right-hand side of (1.1) allows a corresponding limit for R_0 , the dark matter signal, to be calculated for each assumed value of particle mass M_D . Since the Galactic dark matter density and flux are approximately known, the limit on R_0 can be converted to a limit on the particle interaction strength or cross-section. Alternatively, an experiment may determine a limit to the event rate above a specified energy E_1 or in an energy span E_1 to E_2 , in which case the integral of (1.1) above or between these energies again determines a limit to R_0 as a function of M_D . The typical shape of these limits, and their variation with target mass M_T and instrumental energy threshold E_1 , is illustrated in Fig. 1.

In practice, the right-hand side of (1.1) is considerably more complicated, owing to the following corrections:

- The detector is located on the Earth, in orbit around the Sun, with the solar system moving through the Galaxy.
- The detection efficiency for nuclear recoils will in general be different from that for the background electron recoils. Thus the ‘true recoil energy’ will differ from the ‘observed recoil energy’ by that relative efficiency factor.
- The target may consist of more than one element, with separate limits resulting from each.
- There may be instrumental resolution and threshold effects, for example when photomultipliers are used to observe events yielding small numbers of photoelectrons.

- (e) The limits set will in general be different for spin-dependent and spin-independent (scalar) interactions, the latter being, in addition, coherently enhanced in amplitude at low energies by the number of interacting target nucleons.
- (f) There is a form factor correction < 1 which is due to the finite size of the nucleus and dependent principally on nuclear radius and recoil energy. This also differs for spin-dependent and spin-independent interactions.

To take account of these we rewrite (1.1) as

$$\left. \frac{dR}{dE} \right|_{\text{observed}} = R_0 S(E) F^2(E) I \quad (1.2)$$

where S is the modified spectral function taking into account the factors (a-d), F is the form factor correction (f), and I is an interaction function for (e) involving spin-dependent and/or spin-independent factors.

This review concerns the elaboration of (1.1) to include these corrections and to provide convenient practical forms for S and F in (1.2). The quantity R_0 , which remains defined as the unmodified rate for a stationary Earth, can then be estimated from the observed differential spectrum.

These corrections have been discussed in various dark matter papers and reviews [1-12], but not fully covered in any one place; and varying definitions and presentations still give rise to some confusion. As experimental programmes begin to yield new limits, there is now a need to collect the various formulae together in a consistent notation and in a way which facilitates evaluation of proposed new experiments. We also discuss the preferred methods of normalizing results to allow comparison of different experiments and target elements. For future experiments which may incorporate sensitivity to the nuclear recoil direction, we append directional versions of the recoil spectra.

We find it convenient to use an abbreviated notation for the units for event and background rates. It has become conventional to express the unit differential rate as 1 event $\text{keV}^{-1}\text{kg}^{-1}\text{d}^{-1}$, and we refer to this simply as the '*differential rate unit*' (dru). Integrated over energy, the unit for total rate R_0 is 1 event $\text{kg}^{-1}\text{d}^{-1}$, which we refer to as a '*total rate unit*' (tru). In some experiments it is necessary to utilize the partial integral of the differential spectrum between two selected values of E_R . This is also in events $\text{kg}^{-1}\text{d}^{-1}$ but we refer to it as an '*integrated rate unit*' (iru) to distinguish it from the total integral R_0 (tru).

2. Particle density and velocity distribution

Differential particle density is given by:

$$dn = \frac{n_0}{k} f(\mathbf{v}, \mathbf{v}_E) d^3\mathbf{v}$$

where k is a normalization constant such that

$$\int_0^{v_{\text{esc}}} dn \equiv n_0,$$

i.e.,

$$k = \int_0^{2\pi} d\phi \int_{-1}^{+1} d(\cos \theta) \int_0^{v_{\text{esc}}} f(\mathbf{v}, \mathbf{v}_E) v^2 dv.$$

Here n_0 is the mean dark matter particle number density ($= \rho_D/M_D$ for dark matter particle mass M_D , density ρ_D), \mathbf{v} is velocity onto the (Earth-borne) target, \mathbf{v}_E is Earth (target) velocity relative to the dark matter

distribution, and v_{esc} is the local Galactic escape velocity; dn is then the particle density of dark matter particles with relative velocities within d^3v about \mathbf{v} .

We assume a Maxwellian dark matter velocity distribution:

$$f(\mathbf{v}, \mathbf{v}_E) = e^{-(\mathbf{v} + \mathbf{v}_E)^2/v_0^2};$$

then, for $v_{\text{esc}} = \infty$,

$$k = k_0 = (\pi v_0^2)^{3/2}; \quad (2.1)$$

whereas the same distribution truncated¹ at $|\mathbf{v} + \mathbf{v}_E| = v_{\text{esc}}$ would give

$$k = k_1 = k_0 \left[\text{erf} \left(\frac{v_{\text{esc}}}{v_0} \right) - \frac{2}{\pi^{1/2}} \frac{v_{\text{esc}}}{v_0} e^{-v_{\text{esc}}^2/v_0^2} \right]; \quad (2.2)$$

so $k_1 \rightarrow k_0$ as $v_{\text{esc}} \rightarrow \infty$. Derivations of these and subsequent results are given in Appendix A. For $v_0 = 230 \text{ km s}^{-1}$, $v_{\text{esc}} = 600 \text{ km s}^{-1}$ (see Appendix B), we obtain $k_0/k_1 = 0.9965$.

Estimates for ρ_D for a spherical halo have been in the range $0.2 \text{ GeV}c^{-2} \text{ cm}^{-3} \leq \rho_D \leq 0.4 \text{ GeV}c^{-2} \text{ cm}^{-3}$, leading to the adoption of $\rho_D = 0.3 \text{ GeV}c^{-2} \text{ cm}^{-3}$ as the central value. However, it has always been recognized that some flattening of the halo is likely, which would increase ρ_D in the vicinity of the Galactic plane. The most recent estimate is that of Gates et al. [13] who obtain $0.3 \text{ GeV}c^{-2} \text{ cm}^{-3} \leq \rho_D \leq 0.7 \text{ GeV}c^{-2} \text{ cm}^{-3}$ for the total (local) dark matter density in the flattened halos which best model observations, together with an estimated (1995) observational limit of 5–30% for dark matter in the form of non-luminous stars ('MACHOs'). This suggests a value of $\rho_D = 0.4 \text{ GeV}c^{-2} \text{ cm}^{-3}$ for the non-baryonic component at the position of the solar system, subject to any further changes in the estimated MACHO fraction.

3. Basic event rates and energy spectra

The event rate per unit mass on a target of atomic mass A AMU, with cross-section per nucleus σ is

$$dR = \frac{N_0}{A} \sigma v dn,$$

where N_0 is the Avogadro number ($6.02 \cdot 10^{26} \text{ kg}^{-1}$). In this section, we give the total event rates and energy spectra in the absence of the practical corrections discussed in Section 5 and of the form factor corrections discussed in Section 4—i.e., rates for the 'zero momentum transfer' cross-section $\sigma = \text{constant} = \sigma_0$. Then:

$$R = \frac{N_0}{A} \sigma_0 \int v dn \equiv \frac{N_0}{A} \sigma_0 n_0(v).$$

We define R_0 as the event rate per unit mass for $v_E = 0$ and $v_{\text{esc}} = \infty$; i.e.:

$$R_0 = \frac{2}{\pi^{1/2}} \frac{N_0}{A} \frac{\rho_D}{M_D} \sigma_0 v_0 \quad (3.1)$$

(substituting for n_0); so that

$$R = R_0 \frac{\pi^{1/2}}{2} \frac{\langle v \rangle}{v_0}$$

¹ Strictly, the Maxwellian distribution should be modified by a gravitational potential appropriate to v_{esc} ; however, since k_1 above differs from k_0 by less than 0.5%, the errors are not likely to be significant.

$$= R_0 \frac{k_0}{k} \frac{1}{2\pi v_0^4} \int v f(v, v_E) d^3 v.$$

We shall use this result later in differential form:

$$dR = R_0 \frac{k_0}{k} \frac{1}{2\pi v_0^4} v f(v, v_E) d^3 v. \quad (3.2)$$

Then:

$$\frac{R(0, v_{\text{esc}})}{R_0} = \frac{k_0}{k_1} \left[1 - \left(1 + \frac{v_{\text{esc}}^2}{v_0^2} \right) e^{-v_{\text{esc}}^2/v_0^2} \right]; \quad (3.3)$$

$$\frac{R(v_E, \infty)}{R_0} = \frac{1}{2} \left[\pi^{1/2} \left(\frac{v_E}{v_0} + \frac{1}{2} \frac{v_0}{v_E} \right) \text{erf} \left(\frac{v_E}{v_0} \right) + e^{-v_E^2/v_0^2} \right]; \quad (3.4)$$

$$\frac{R(v_E, v_{\text{esc}})}{R_0} = \frac{k_0}{k_1} \left[\frac{R(v_E, \infty)}{R_0} - \left(\frac{v_{\text{esc}}^2}{v_0^2} + \frac{1}{3} \frac{v_E^2}{v_0^2} + 1 \right) e^{-v_{\text{esc}}^2/v_0^2} \right]. \quad (3.5)$$

Again taking $v_0 = 230 \text{ km s}^{-1}$, $v_{\text{esc}} = 600 \text{ km s}^{-1}$, we obtain: $R(0, v_{\text{esc}})/R_0 = 0.9948$. The Earth velocity $v_E \sim v_0$, but varies during the year as the Earth moves round the Sun (Appendix B). For practical purposes,

$$v_E \simeq 244 + 15 \sin(2\pi y) \text{ km s}^{-1}, \quad (3.6)$$

where y is the elapsed time from (approximately) March 2nd, in years.

Note that, while the mean level is uncertain by $\sim 20 \text{ km s}^{-1}$ (from galactic motion uncertainty), the modulation amplitude has negligible uncertainty; however, use of the above expression gives rise to small errors since the modulation is not exactly sinusoidal. The $\sim 6\%$ velocity modulation in (3.6) gives rise to a $\sim 3\%$ modulation in rate (this can be seen by differentiating (3.4), yielding

$$\begin{aligned} \frac{d}{dv_E} \left(\frac{R}{R_0} \right) &= \frac{1}{v_E} \left[\frac{R}{R_0} - \frac{\pi^{1/2} v_0}{2v_E} \text{erf} \left(\frac{v_E}{v_0} \right) \right], \\ &\sim \frac{1}{2v_E} \frac{R}{R_0} \quad \text{for } v_E \sim v_0. \end{aligned}$$

Physically, mean velocity onto target, $\propto R$, is both larger than the mean of v_E and varies less than v_E . However, because the modulation in dR/dE_R changes sign with energy (see Fig. 2), modulation of the sum of the absolute differences in binned data is significantly larger (dependent on energy threshold)—see also Table 1. The effect would be further enhanced by a statistical analysis with respect to energy.

R_0 is conventionally expressed in units $\text{kg}^{-1}\text{d}^{-1}$, or ‘tru’ (see Section 1). Normalized to $\rho_D = 0.4 \text{ GeVc}^{-2} \text{ cm}^{-3}$ and $v_0 = 230 \text{ km s}^{-1}$, (3.1) becomes:

$$\begin{aligned} R_0 &= \frac{540}{AM_D} \left(\frac{\sigma_0}{1 \text{ pb}} \right) \left(\frac{\rho_D}{0.4 \text{ GeVc}^{-2} \text{ cm}^{-3}} \right) \left(\frac{v_0}{230 \text{ km s}^{-1}} \right) \text{tru} \\ &= \frac{503}{M_D M_T} \left(\frac{\sigma_0}{1 \text{ pb}} \right) \left(\frac{\rho_D}{0.4 \text{ GeVc}^{-2} \text{ cm}^{-3}} \right) \left(\frac{v_0}{230 \text{ km s}^{-1}} \right) \text{tru} \end{aligned} \quad (3.7)$$

with M_D, M_T in GeVc^{-2} ($M_T = 0.932 A$, is the mass of the target nucleus).

The recoil energy of a nucleus struck by a dark matter particle of kinetic energy $E = \frac{1}{2} M_D v^2 = \frac{1}{2} M_D c^2 (v/c)^2$, scattered at angle θ (in centre-of-mass) is:

$$E_R = E r (1 - \cos \theta) / 2$$

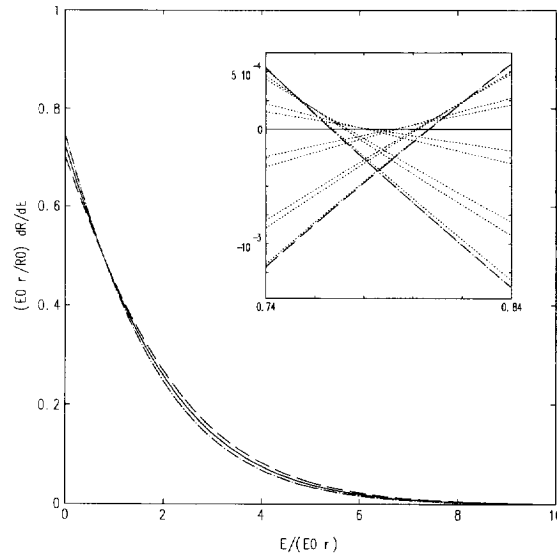


Fig. 2. Seasonal variation of rate spectrum; — annual average, - - - June, - - - - December. *Inset:* enlargement of cross-over region, annual average subtracted. ····· monthly averages.

where

$$r = 4M_D M_T / (M_D + M_T)^2. \quad (3.8)$$

We assume the scattering is isotropic, i.e. uniform in $\cos \theta$, so that recoils are uniformly distributed in E_R , over the range $0 \leq E_R \leq Er$; hence

$$\begin{aligned} \frac{dR}{dE_R} &= \int_{E_{\min}}^{E_{\max}} \frac{1}{Er} dR(E) \\ &= \frac{1}{E_0 r} \int_{v_{\min}}^{v_{\max}} \frac{v_0^2}{v^2} dR(v), \end{aligned}$$

where $E_{\min} = E_R/r$, the smallest particle energy which can give a recoil energy of E_R ; $E_0 = \frac{1}{2} M_D v_0^2 = (v_0^2/v^2) E$; and v_{\min} is the dark matter particle velocity corresponding to E_{\min} , i.e.,

$$v_{\min} = (2E_{\min}/M_D)^{1/2} = (E_R/E_0 r)^{1/2} v_0.$$

So, using (3.2), we have:

$$\frac{dR}{dE_R} = \frac{R_0}{E_0 r} \frac{k_0}{k} \frac{1}{2\pi v_0^2} \int_{v_{\min}}^{v_{\max}} \frac{1}{v} f(v, v_E) d^3 v, \quad (3.9)$$

from which we obtain:

$$\frac{dR(0, \infty)}{dE_R} = \frac{R_0}{E_0 r} e^{-E_R/E_0 r}, \quad (3.10)$$

which is the basic unmodified nuclear recoil spectrum for $v_E = 0$ already referred to in Section 1.

With non-zero v_E and finite v_{esc} , (3.9) gives:

$$\begin{aligned} \frac{dR(0, v_{\text{esc}})}{dE_R} &= \frac{k_0}{k_1} \frac{R_0}{E_0 r} \left(e^{-E_R/E_0 r} - e^{-v_{\text{esc}}^2/v_0^2} \right) \\ &= \frac{k_0}{k_1} \left[\frac{dR(0, \infty)}{dE_R} - \frac{R_0}{E_0 r} e^{-v_{\text{esc}}^2/v_0^2} \right]; \end{aligned} \quad (3.11)$$

$$\frac{dR(v_E, \infty)}{dE_R} = \frac{R_0}{E_0 r} \frac{\pi^{1/2}}{4} \frac{v_0}{v_E} \left[\text{erf} \left(\frac{v_{\min} + v_E}{v_0} \right) - \text{erf} \left(\frac{v_{\min} - v_E}{v_0} \right) \right]; \quad (3.12)$$

$$\frac{dR(v_E, v_{\text{esc}})}{dE_R} = \frac{k_0}{k_1} \left[\frac{dR(v_E, \infty)}{dE_R} - \frac{R_0}{E_0 r} e^{-v_{\text{esc}}^2/v_0^2} \right]. \quad (3.13)$$

June, December, and annual averages of (3.13) are shown in Fig. 2 for $v_0 = 230 \text{ km s}^{-1}$, $v_{\text{esc}} = 600 \text{ km s}^{-1}$, with v_E from (3.6). The inset is an enlargement of the cross-over region— $E_R \sim 0.78 E_0 r$ —for these velocities, showing differences between mean monthly rates and the annual average.

For practical purposes, $dR(v_E, \infty)/dE_R$ is well approximated by:

$$\frac{dR(v_E, \infty)}{dE_R} = c_1 \frac{R_0}{E_0 r} e^{-c_2 E_R/E_0 r}, \quad (3.14)$$

where c_1, c_2 are fitting constants, of order unity. Values of c_1, c_2 for different months and energy thresholds are discussed in Appendix C. Note that c_1, c_2 are not independent: by integration,

$$\frac{c_1}{c_2} = \frac{R(v_E, \infty)}{R_0}.$$

For most purposes it is sufficient to take fixed average values $c_1 = 0.751$, $c_2 = 0.561$.

dR/dE_R is conventionally expressed in units $\text{keV}^{-1} \text{kg}^{-1} \text{d}^{-1}$, or ‘dru’ (see Section 1).

For some types of experiment, the data may yield a limit on the total number of events in a finite energy range, or the total above some minimum energy. For these cases we need the integrated form of (3.14):

$$R(E_1, E_2) = R_0 \frac{c_1}{c_2} \left[e^{-c_2 E_1/E_0 r} - e^{-c_2 E_2/E_0 r} \right] \quad (3.15)$$

giving the integrated rate over a recoil energy range $E_R = E_1$ to $E_R = E_2$. In practice, (3.14) and (3.15) are modified to take account of a form factor, as discussed in the next section.

As observed in Section 1, it is helpful to refer to the units of (3.15) ($\text{kg}^{-1} \text{d}^{-1}$) as ‘integrated rate units’ (iru), reserving ‘tru’ specifically for the total integral $E_1 = 0$, $E_2 = \infty$. Note that the total rate from (3.15) is $(c_1/c_2) \times R_0 \sim 1.3 \times R_0$, varying with time of year as discussed above. R_0 remains defined as the time-independent rate corresponding to zero Galactic velocity ($v_E = 0$).

Spergel [14] has derived the differential angular spectrum ($v_{\text{esc}} = \infty$) with respect to laboratory recoil angle ψ ; in our notation:

$$\frac{d^2 R(v_E, \infty)}{dE_R d(\cos \psi)} = \frac{1}{2} \frac{R_0}{E_0 r} e^{-(v_E \cos \psi - v_{\min})^2/v_0^2}. \quad (3.16)$$

In Appendix A we show that integration of this with respect to $\cos \psi$ correctly yields our result for $dR(v_E, \infty)/dE_R$; carrying out the integration separately over the forward ($0 \leq \cos \psi \leq 1$) and backward hemispheres yields:

$$\frac{dR(v_E, \infty)}{dE_R} \Big|_{\text{forward}} = \frac{R_0}{E_0 r} \frac{\pi^{1/2}}{4} \frac{v_0}{v_E} \left[\text{erf} \left(\frac{v_{\min}}{v_0} \right) - \text{erf} \left(\frac{v_{\min} - v_E}{v_0} \right) \right];$$

$$\frac{dR(v_E, \infty)}{dE_R} \Big|_{\text{backward}} = \frac{R_0}{E_0 r} \frac{\pi^{1/2}}{4} \frac{v_0}{v_E} \left[\text{erf} \left(\frac{v_{\min} + v_E}{v_0} \right) - \text{erf} \left(\frac{v_{\min}}{v_0} \right) \right].$$

Clearly, these sum to (3.12). Rates in the energy bin $E_1 \leq E_R \leq E_2$, $R(E_1, E_2)|_{\text{forward, backward}}$, can be obtained by numerical integration.

Table 1 illustrates both seasonal and directional variation in binned rates, all obtained by numerical integration of the exact differential formulae.

Some 'directional' detection ideas would only give directional information modulo π —i.e. would give the angle between recoil path and target trajectory but not the direction of recoil along that path. In such cases, it may only be possible to look for the smaller asymmetry between rates resolved parallel and perpendicular to the target trajectory:

$$\frac{dR(v_E, \infty)}{dE_R} \Big|_{\parallel} = \int_{-1}^1 |\cos \psi| \frac{d^2 R(v_E, \infty)}{dE_R d(\cos \psi)} d(\cos \psi),$$

$$\frac{dR(v_E, \infty)}{dE_R} \Big|_{\perp} = \int_{-1}^1 (1 - \cos^2 \psi)^{1/2} \frac{d^2 R(v_E, \infty)}{dE_R d(\cos \psi)} d(\cos \psi).$$

Though the integral for the parallel component can be evaluated analytically, it will usually be more appropriate to integrate (3.16) with respect to E_R over an energy bin, obtaining:

$$\frac{1}{R_0} \frac{dR(v_E, \infty)}{d(\cos \psi)} = \frac{1}{2} \left[e^{-(v_1 - v_E \cos \psi)^2/v_0^2} - e^{-(v_2 - v_E \cos \psi)^2/v_0^2} \right] + \frac{\pi^{1/2}}{2} \frac{v_E}{v_0} \cos \psi \left[\text{erf} \left(\frac{v_2 - v_E \cos \psi}{v_0} \right) - \text{erf} \left(\frac{v_1 - v_E \cos \psi}{v_0} \right) \right], \quad (3.17)$$

with $v_{1,2} = (E_{1,2}/E_0 r)^{1/2} v_0$.

$R(E_1, E_2)_{\parallel}, R(E_1, E_2)_{\perp}$ are then obtained by numerical integration of (3.17); Table 2 gives values for the same binnings as in Table 1.

4. Nuclear form factor correction

When the momentum transfer $q = (2M_T E_R)^{1/2}$, is such that the wavelength h/q is no longer large compared to the nuclear radius, the effective cross-section begins to fall with increasing q , even in the case of spin-dependent scattering which effectively involves a single nucleon (for a particularly clear statement, see [15]). It is convenient, and usually adequate, to represent this by a 'form factor', F , which is a function of the dimensionless quantity qr_n/\hbar where r_n is an effective nuclear radius. In the following we use units in which $\hbar = 1$, so that 'qr_n' is this dimensionless quantity.

With r_n approximated by $r_n = a_n A^{1/3} + b_n$, and with

$$q(\text{MeV}c^{-1}) = [2 \times 0.932(\text{GeV}c^{-2}) A E_R(\text{keV})]^{1/2},$$

we have, since $\hbar = 197.3$ MeV fm:

$$qr_n \text{ (dimensionless)} = 6.92 \times 10^{-3} A^{1/2} E_R^{1/2} (a_n A^{1/3} + b_n) \quad (4.1)$$

Table 1
Energy dependence of annual modulation and forward/back ratios

energy range E_R/E_0r	normalized total rate R/R_0				directional components of R/R_0					
	Jun		abs (Jun)		June			December		
	Jun	Dec	– Dec	– Dec	forward	back	ratio	forward	back	ratio
0.0-0.1	0.069	0.073	–0.0043	0.0043	0.041	0.028	1.46	0.043	0.030	1.42
0.1-0.2	0.066	0.069	–0.0035	0.0035	0.044	0.022	2.02	0.046	0.024	1.92
0.2-0.3	0.063	0.066	–0.0028	0.0028	0.045	0.018	2.48	0.046	0.020	2.33
0.3-0.5	0.118	0.122	–0.0037	0.0037	0.090	0.028	3.16	0.091	0.031	2.91
0.5-0.7	0.108	0.110	–0.0016	0.0016	0.087	0.021	4.12	0.086	0.023	3.71
0.7-1.0	0.144	0.144	0.0007	0.0007	0.122	0.022	5.41	0.119	0.025	4.77
1-2	0.352	0.335	0.0166	0.0166	0.317	0.035	9.09	0.297	0.039	7.67
2-3	0.206	0.184	0.0220	0.0220	0.195	0.011	18.5	0.173	0.012	14.6
3-5	0.179	0.148	0.0308	0.0308	0.174	0.005	38.5	0.144	0.005	28.5
5-7	0.051	0.038	0.0127	0.0127	0.050	0.0005	99.0	0.038	0.0006	66.7
7-10	0.016	0.011	0.0050	0.0050	0.016	0.00007	237.	0.011	0.00007	146.
total	1.374	1.302	0.0727	0.1046	1.183	0.191	6.20	1.094	0.209	5.23

Table 2
Energy dependence of parallel/perpendicular ratios

energy range E_R/E_0r	resolved components of R/R_0								
	June			December			Annual average		
	parallel	\perp	ratio	parallel	\perp	ratio	parallel	\perp	ratio
0.0-0.1	0.028	0.058	0.49	0.031	0.061	0.51	0.030	0.060	0.50
0.1-0.2	0.028	0.055	0.51	0.031	0.057	0.54	0.030	0.056	0.52
0.2-0.3	0.028	0.052	0.54	0.030	0.054	0.56	0.029	0.053	0.55
0.3-0.5	0.055	0.096	0.57	0.058	0.098	0.59	0.056	0.097	0.58
0.5-0.7	0.053	0.086	0.62	0.054	0.087	0.63	0.054	0.086	0.62
0.7-1.0	0.075	0.112	0.67	0.075	0.111	0.67	0.075	0.112	0.67
1-2	0.201	0.258	0.78	0.191	0.246	0.77	0.196	0.252	0.78
2-3	0.131	0.140	0.94	0.116	0.126	0.92	0.124	0.133	0.93
3-5	0.124	0.112	1.11	0.102	0.095	1.08	0.113	0.103	1.10
5-7	0.038	0.029	1.32	0.028	0.022	1.26	0.033	0.026	1.29
7-10	0.012	0.0082	1.50	0.0084	0.0058	1.43	0.010	0.0070	1.47
total	0.777	1.007	0.77	0.725	0.965	0.75	0.751	0.987	0.76

with E_R in keV and a, b in fm.

Cross-sections then behave as:

$$\sigma(qr_n) = \sigma_0 F^2(qr_n),$$

where σ_0 is the cross-section at zero momentum transfer. Separation into one term (σ_0) containing all dependence on the specific interaction and a second ($F(qr_n)$) dependent only on momentum transfer is convenient in allowing results to be presented in an almost model-independent fashion. It must be noted, however, that, in the case of spin-dependent interactions, this corresponds to considering contributions from only the unpaired nucleon (the 'single-particle' model) or nucleons of the same type as the unpaired nucleon (the 'odd-group'

model), and is likely to be substantially in error for large mass nuclei [11].

In the first Born (plane wave) approximation, the form factor is the Fourier transform of $\rho(r)$, the density distribution of the ‘scattering centres’:

$$\begin{aligned} F(q) &= \int \rho(r) e^{iq \cdot r} d^3 r \\ &= \int_0^{2\pi} d\phi \int_r^{\infty} r^2 \rho(r) \int_{-1}^{+1} e^{iqr \cos \theta} d(\cos \theta) dr \\ &= \frac{4\pi}{q} \int_0^{\infty} r \sin qr \rho(r) dr. \end{aligned}$$

A useful starting point is to consider the form factors obtained by Fourier transform of (a) a thin shell, approximating a single outer shell nucleon for the case of spin-dependent interactions², and (b) a solid sphere, approximating spin-independent interaction with the whole nucleus. The results are:

(a) thin shell:

$$F(qr_n) = j_0(qr_n) = \sin(qr_n)/qr_n; \quad (4.2)$$

(b) solid sphere:

$$F(qr_n) = 3j_1(qr_n)/qr_n = 3[\sin(qr_n) - qr_n \cos(qr_n)]/(qr_n)^3. \quad (4.3)$$

A commonly used approximation is:

$$F^2(qr_n) = e^{-\alpha(qr_n)^2}; \quad (4.4)$$

with $\alpha = 1/3$, this is the exact form factor for a Gaussian scatterer of $r_{\text{rms}} = r_n$ (see [11,24]); for small qr_n , this is an adequate approximation to (4.2). $\alpha = 1/5$ gives a comparable fit to (4.3) (see Figs. 3 and 4), but clearly poor fits result for qr_n much beyond 3–4.

In the spin-dependent case, the more exact computations of Engel et al. [11] show that, when coupling to all ‘odd-group’ nucleons is taken into account, the (early) zeros of the Bessel function (4.2) are at least partially filled (see Fig. 3). For the experimentally useful range $0 < qr_n \leq 6$, these results are adequately approximated by (4.2) with F^2 replaced across the first dip by its value at the second maximum:

$$\begin{aligned} F^2(qr_n) &= \begin{cases} j_0^2(qr_n) & (qr_n < 2.55, qr_n > 4.5), \\ \text{constant} \simeq 0.047 & (2.55 \leq qr_n \leq 4.5); \end{cases} \\ r_n &\simeq 1.0A^{1/3} \text{ fm}. \end{aligned} \quad (4.5)$$

For the spin-independent case the distribution of WIMP scatterers is assumed to be the same as the charge distribution derived from experimental data for electron [17] and muon scattering (the latter is comprehensively reviewed in [18]). The essential change from the uniform distribution yielding (4.3) is the appearance of a ‘soft edge’—charge density falling to zero over a finite skin thickness, resulting in an effective damping of the form factor. In electron and muon scattering, the Bessel function zeros are again partially filled (increasingly so as A increases); but, as this is essentially due to multiple photon exchange in the nucleus, it is not expected in the WIMP case [19].

² But note that this may be a poor approximation if the odd nucleon is not in an *s*-state [16].

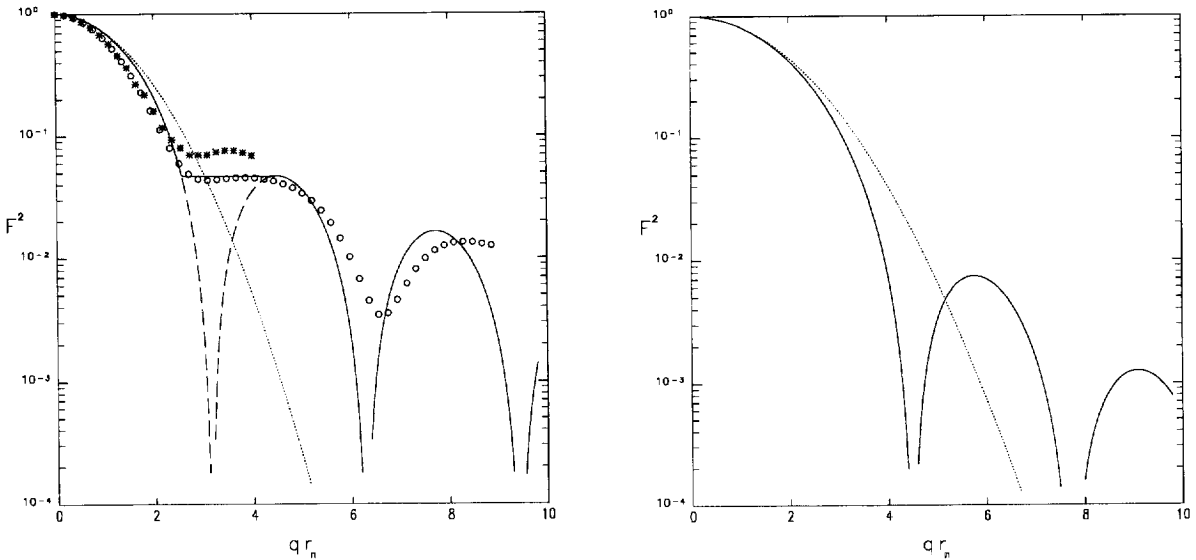


Fig. 3. Form factor, thin shell approximation; $\exp[-(qr_n)^{2/3}/3]$, - - - $[\sin(qr_n)/qr_n]^2$ (thin shell), —— approximate fit, o o o o o ^{131}Xe (Engel et al., single-particle model), * * * * * Nb (Engel et al., single-particle model).

Fig. 4. Form factor, solid sphere approximation; $\exp[-(qr_n)^{2/3}/5]$, —— $\{3[\sin(qr_n) - qr_n \cos(qr_n)]/(qr_n)^3\}^2$ (solid sphere).

Numerous multi-parameter fits to charge density have been proposed [17,20]; form factors are not particularly sensitive to the details of the fit, but the most realistic is generally considered to be the Fermi distribution:

$$\rho(r) = \rho_0 \left[1 + \exp \left(\frac{r - c}{a} \right) \right]^{-1}. \quad (4.6)$$

The distribution proposed by Helm [21], however, has the advantage of yielding an analytic form factor expression:

$$F(qr_n) = 3 \frac{j_1(qr_n)}{qr_n} \times e^{-(qs)^2/2}, \quad (4.7)$$

where s is a measure of the nuclear skin thickness. Numerical integration of the Fermi distribution yields very similar results.

The parameters in (4.6), (4.7) are determined from experimental estimates of r_{rms} in conjunction with the observation that skin thickness is essentially constant. For a uniform sphere of radius r_n ,

$$r_{\text{rms}}^2 = \frac{3}{5} r_n^2;$$

for (4.6) [22],

$$r_{\text{rms}}^2 = \frac{3}{5} c^2 + \frac{7}{5} \pi^2 a^2; \quad (4.8)$$

and for (4.7),

$$r_{\text{rms}}^2 = \frac{3}{5} r_n^2 + 3s^2. \quad (4.9)$$

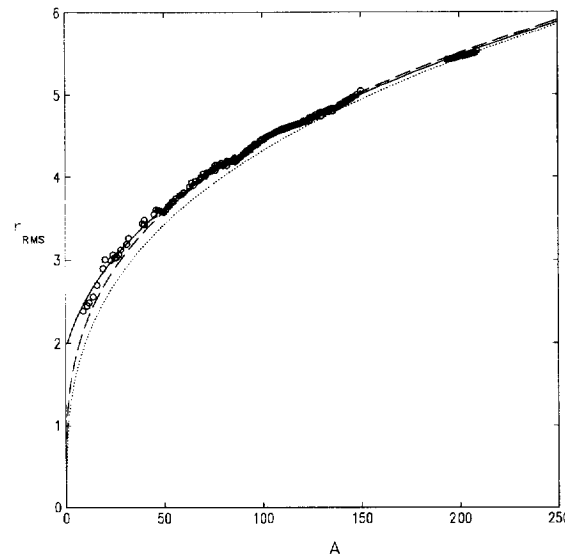


Fig. 5. Nuclear rms charge radii: o o o o o muon data [18], — least-squares fit to c , ····· Engel [15] fit, - - - Eder [23] fit.

For thickness parameter, Engel [15] takes $s \sim 1$ fm in (4.7) while Fricke et al. [18] use a 10–90% thickness of 2.30 fm ($a \simeq 0.52$ fm) in fitting muon scattering data to (4.6); and, for r_{rms} , commonly used approximations are $r_{\text{rms}} \sim A^{1/3}$ fm or, with rather greater precision, $r_{\text{rms}} \simeq 0.89A^{1/3} + 0.30$ fm [23]. Such approximations have the slight disadvantage of resulting in significant errors at small A ; we prefer to use a two-parameter least-squares fit to the Fricke et al. compilation of c in (4.6):

$$c \simeq 1.23A^{1/3} - 0.60 \text{ fm}; \quad (4.10)$$

then, from (4.8) and (4.9), r_n for (4.7) is obtained from:

$$r_n^2 = c^2 + \frac{7}{3}\pi^2 a^2 - 5s^2. \quad (4.11)$$

Data from [18], and the various fits to r_{rms} are shown in Fig. 5.

We find $s \simeq 0.9$ fm improves the match between Helm and numerically integrated Fermi distributions (see Figs. 6, 7); and, for most A , (4.11) is well fitted by $r_n \simeq 1.14A^{1/3}$. Figs. 8 and 9 show the Na and I form factor dependence on E_R , illustrating the limitation of large A materials. Moreover, as discussed in Section 5.1 below, in detectors based on scintillation or ionization the observed apparent energy E_v is less than E_R by an A -dependent ‘relative efficiency’ f_n ; the range of E_R shown corresponds to $E_v \simeq 0$ –310 keV for Na, but only $\simeq 0$ –90 keV for I.

More precise calculations have been carried out in the spin-dependent case for a small number of nuclei [11,12]. In these calculations, which include contributions from all the nucleons, the form factor has three parts, which can be represented as due to proton, neutron, and interference terms or to isoscalar ($p + n$), isovector ($p - n$), and interference terms. In the latter representation, $F^2(qr_n) = S(q)/S(0)$, where:

$$S(q) = a_0^2 S_{00}(q) + a_1^2 S_{11}(q) + a_0 a_1 S_{01}(q);$$

the S_{ij} are computed using the shell model of the specific nucleus; and the isoscalar (a_0) and isovector (a_1) coefficients are related to the WIMP-nucleon spin factors discussed in Section 6 below: $a_0 \propto C_{Wp} + C_{Wn}$; $a_1 \propto C_{Wp} - C_{Wn}$.

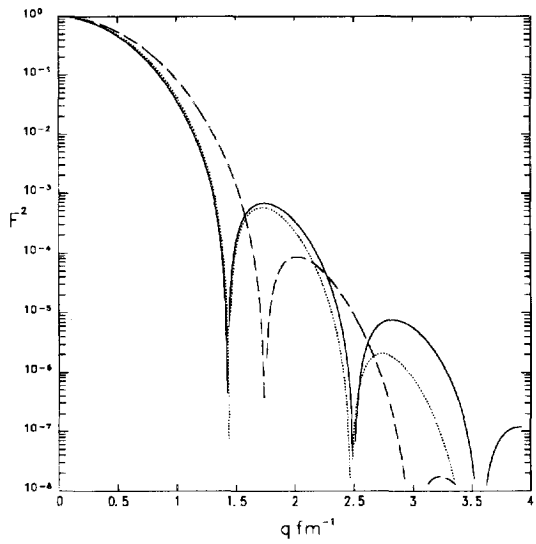


Fig. 6. Form factor versus q for Na. ——— Fermi density, data from [18]. ····· Helm density: r_n from (4.10), (4.11); $s = 0.9$ fm. - - - Helm density, Engel [15] fit: $r_{\text{rms}} = 0.93A^{1/3}$; $s = 1.0$ fm.

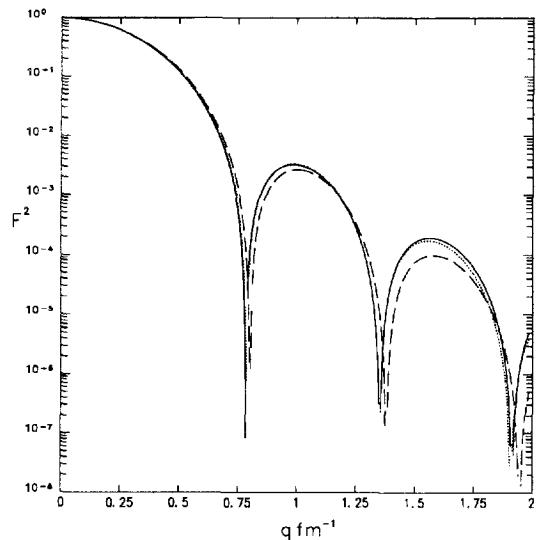


Fig. 7. Form factor versus q for I. Figure legend: same as Fig. 6.

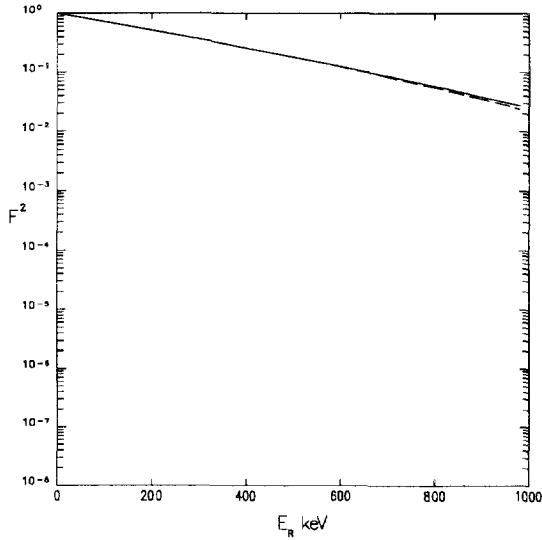


Fig. 8. Form factor versus E_R for Na. ——— Fermi density, data from [18]. - - - Helm density: $r_n = 1.14A^{1/3}$; $s = 0.9$ fm.

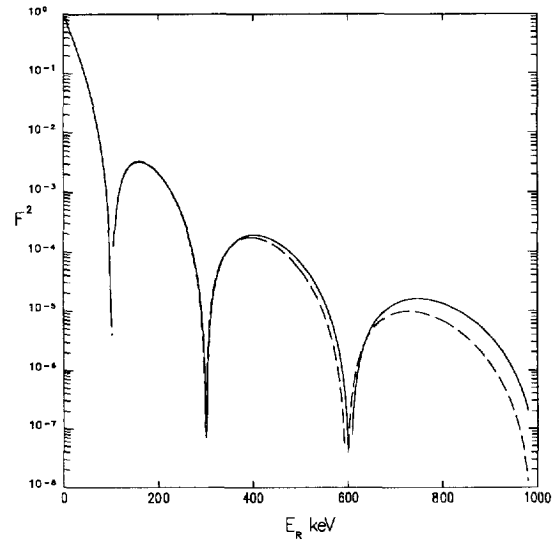


Fig. 9. Form factor versus E_R for I. Figure legend: same as Fig. 8.

Such calculations, where available, should be used to set limits on specific WIMPs.

5. Detector response corrections

The form factor corrected spectra (4.5), (4.7) apply to an ideal detector consisting of a single element, with 100% detection efficiency. In this section we discuss additional corrections which are intrinsic to the detection process and independent of the precise nature of the dark matter interaction.

5.1. Energy detection efficiency

For scintillation and ionization detectors calibrated with γ sources, the apparent observed nuclear recoil energy is less than the true value; the ratio, the ‘relative efficiency’ f_n , is determined by neutron scattering measurements. While this additional calibration factor could, of course, be incorporated to yield observed spectra directly in terms of E_R , experimenters prefer to work with the γ -calibrated energies for easy identification of background γ s. Consequently, E_R in the above rates and spectra should be replaced by the ‘visible’ energy E_v , using $E_R = E_v / f_n$ —and, allowing for possible variation of f_n with E_R ,

$$\frac{dR}{dE_R} = f_n \left(1 + \frac{E_R}{f_n} \frac{df_n}{dE_R} \right) \frac{dR}{dE_v}. \quad (5.1)$$

For ionization detectors, Lindhard et al. [25] represent f_n by

$$f_n = \frac{kg(\varepsilon)}{1 + kg(\varepsilon)} \quad (5.2)$$

where, for a nucleus of atomic no. Z ,

$$\varepsilon = 11.5 E_R(\text{keV}) Z^{-7/3}, \quad k = 0.133 Z^{2/3} A^{1/2},$$

and $g(\varepsilon)$ is well fitted by:

$$g(\varepsilon) = 3\varepsilon^{0.15} + 0.7\varepsilon^{0.6} + \varepsilon.$$

While f_n for scintillation detectors might be expected to behave in a similar fashion, measurements so far show no evidence of significant energy dependence. Neutron scattering measurements give $f_n \sim 0.3, 0.09$ respectively for Na and I in NaI(Tl) [26] and 0.08, 0.12 respectively for Ca and F in CaF₂(Eu) [27], over substantial energy ranges.

One expects a rapid drop in ionization or scintillation efficiency when nuclear recoil energies fall below a threshold value at which the maximum energy transfer to target electrons is less than the necessary excitation energy E_g [28]. This threshold region is expected kinematically at an energy of order

$$E_c = \frac{M_T}{4m_e} \left[(E_e + E_g)^{1/2} - E_e^{1/2} \right]^2 \quad (5.3)$$

for electrons (mass m_e) of characteristic kinetic energy E_e (typically ~ 10 eV). For $E_g \ll E_e$ this approximates to $E_c(\text{keV}) \sim 0.1 A E_g^2 / E_e$ (E_g, E_e in eV). The threshold region can be parameterized by multiplying the relative efficiency by $[1 - \exp(-E_R/E_t)]$. E_t is expected to be ~ 0.3 keV for Ge and Si, but above 1 keV for other crystalline targets. However, it should be emphasized that as yet the only evidence confirming low energy threshold effects comes from plastic scintillator [29], and it may become important to investigate this as practical energy thresholds are improved. Examples of predicted threshold curves are shown in an earlier review [3].

5.2. Energy resolution and threshold cut-off

Finite detector energy resolution means that N recoils at a single energy E' would be observed as a spectrum distributed in approximately Gaussian fashion:

$$\frac{dN(E)}{dE} = \frac{N}{(2\pi)^{1/2}\Delta E} e^{-(E-E')^2/2\Delta E^2},$$

resulting in the transformation:

$$\frac{dR}{dE_v} = \frac{1}{(2\pi)^{1/2}} \int \frac{1}{\Delta E} \frac{dR}{dE'_v} e^{-(E_v-E'_v)^2/2\Delta E^2} dE'_v. \quad (5.4)$$

ΔE is energy dependent: for detectors with linear response, statistical fluctuations alone would give $\Delta E(E') \propto (E')^{1/2}$; additional terms occur in practical detectors [30].

Energy resolution is conventionally expressed as the ratio of peak full width at half maximum to mean energy, $\Delta E_{\text{FWHM}}/E'$, where $\Delta E_{\text{FWHM}} = (8 \ln 2)^{1/2} \Delta E = 2.35 \times \Delta E$.

In general the detector signal may consist of a discrete number of counts $n = E'/\varepsilon$ (e.g. from a photomultiplier) and at low energy this number may be sufficiently small that the Gaussian in (5.4) would lead to erroneous loss of counts to unphysical negative energy. The statistical component of the resolution can be correctly represented by use of Poisson instead of Gaussian statistics:

$$\frac{dR}{dE_v} = \frac{1}{n! \varepsilon} \int \frac{dR}{dE'_v} \left(\frac{E'_v}{\varepsilon} \right)^n e^{-(E'_v/\varepsilon)} dE'_v, \\ E_v = n\varepsilon. \quad (5.5)$$

In such detectors the need to set a threshold to reduce intrinsic rates, often in conjunction with coincidence counting, results in reduced detection efficiency at low energies, dropping to zero at the set threshold.

We illustrate this effect by considering the case of two PMTs run in coincidence, each with the same threshold. If the two PMTs are balanced so that an event produces the same mean number of photoelectrons in each, then, for an event producing n photoelectrons in total, the best estimate of the probability that m ($\leq n$) arrive at one PMT (and hence $n-m$ at the other) is

$$p_{n,2}(m) = K e^{-n/2} (n/2)^m / m!$$

where K is a normalization factor such that $\sum_{m=0}^n p_{n,2}(m) \equiv 1$; thus:

$$p_{n,2}(m) = \frac{(n/2)^m / m!}{\sum_{k=0}^n (n/2)^k / k!}.$$

Then, for coincidence counting with a threshold of $\geq n_t$ photoelectrons in each PMT, only those events for which $n_t \leq m \leq n - n_t$ (in each PMT) are accepted. Hence the counting efficiency is

$$\eta(n, n_t) = \frac{\sum_{m=n_t}^{n-n_t} (n/2)^m / m!}{\sum_{m=0}^n (n/2)^m / m!}. \quad (5.6)$$

An approximate analytic fit to this is:

$$\eta(n, n_t) \approx 1 - \exp \left[\frac{-2(n - 2n_t)^{1.5}}{n} \right] \quad (5.7)$$

Depending on particular experimental circumstances, one of two possible approaches may be adopted in compensating for these effects:

- (a) The intrinsic dark matter spectrum (3.13) is transformed using (5.4) or (5.5) and the result multiplied by (5.6), to give (together with the other corrections discussed in Section 4 and Section 6) a corresponding observable spectrum. Standard statistical procedures can then be used to determine limits on R_0 consistent with the actual observed spectrum [32,31].
- (b) An approximation to the original spectrum is obtained by an iterative search for a spectrum which, when subject to the transformation (5.4) or (5.5), yields a good fit to the observed spectrum (divided by (5.6)). Since low data rates mean that it is normally both necessary and desirable to work with fairly coarsely binned data, it is reasonable to represent the original spectrum by a suitable smooth function with 2–3 variable parameters which are adjusted for best fit [33].

5.3. Target mass fractions

For compound targets, it is usual to extract a limit on R_0 separately for each element. The differential rate in equations of the form (1.2) is defined per kg of the whole target. If the counts are attributed to element A which contributes a fraction f_A of the target mass, then R_0 per kg of A is obtained by rewriting (1.2) as

$$\frac{1}{f_A} \frac{dR}{dE} \Big|_{\text{observed}} = R_0 S_A F_A^2 I_A,$$

i.e.

$$\frac{dR}{dE} \Big|_{\text{observed}} = f_A R_0 S_A F_A^2 I_A. \quad (5.8)$$

If the elemental dependence of the interaction is understood theoretically, then the more accurate procedure can be adopted of retaining R_0 as the total rate and writing (1.2) as the sum of n terms for the n constituent elements:

$$\frac{dR}{dE} \Big|_{\text{observed}} = R_0 \sum_A f_A S_A F_A^2 I_A \quad (5.9)$$

allowing the total R_0 to be calculated from the observed spectrum. The A -dependence of the form factor F (via the nuclear radius) has been discussed in Section 4. The A -dependence of the spectral function S arises through the kinematic factor r (Section 3) and also through the nuclear recoil efficiency f_n (Section 5.1). The final factor, I , representing the spin-dependence and/or coherence of the interaction, is discussed in the next section, and used to convert R_0 to a basic ‘WIMP-nucleon’ cross-section σ_{WN} . Note that if such a cross-section limit is determined separately from (5.8) for each element, an improved combined limit can be obtained using (5.9) together with $\sum f_A \equiv 1$:

$$\frac{1}{\sigma_{WN}} = \sum_A \frac{1}{\sigma_{WN}(A)}. \quad (5.10)$$

6. Interaction factor—spin-dependence

6.1. Spin-independent ('coherent') interactions

For the simplest case of interactions which are independent of spin and the same for neutrons and protons, there will be A scattering amplitudes which, for sufficiently low momentum transfer ($qr_n \ll 1$), would add in phase to give a coherent cross-section $\propto A^2$.

In this situation we can define R_0 as the rate corresponding to a single nucleon, multiplied by a coherent interaction factor $I_c \equiv A^2$ in (1.2). Rates or cross-sections for different target elements should thus be divided by the corresponding A^2 to normalize each to the case $A = 1$.

In practice the situation can be more complicated, as illustrated by the known example of heavy (non-relativistic) Dirac neutrinos, for which the coherent cross-section is [2]

$$\sigma_{\nu_D(\text{coh.})} = \frac{G_F^2}{8\pi\hbar^4} \mu^2 I_c \quad (6.1)$$

i.e., with $\hbar c = 0.197$ GeV fm and $G_F/(\hbar c)^3 = 1.166 \text{ GeV}^{-2}$,

$$\sigma_{\nu_D(\text{coh.})}(\text{pb}) = 2.11 \cdot 10^{-3} \mu^2 I_c$$

where $\mu(\text{GeV}c^{-2})$ is the reduced mass of neutrino + target nucleus and $I_c = N_1^2$, $N_1 = (A - Z) + \epsilon Z$, $\epsilon = (1 - 4 \sin^2 \theta_W) \sim 0.08$. Thus the Weinberg–Salam factor results in a proportionality to approximately the square of the number of neutrons, $I_c \sim (A - Z)^2$, rather than $I_c = A^2$. Nevertheless, normalization of rates by either $(A - Z)^2$ or A^2 will always provide a reasonable method of comparing results from different targets. This is of particular importance in the planning of new experiments, to give a realistic assessment of the lighter elements for spin-independent interactions.

Note that the coherence is lost as the momentum transfer increases ($qr_n \gtrsim 1$) since the scattering amplitudes no longer add in phase. This is taken account of by the form factor correction F in (1.2), already discussed in Section 4.

The hypothetical neutrino superpartner (sneutrino) would have a cross-section four times that of (6.1) [2].

6.2. Spin-dependent interactions

For spin-dependent interactions the scattering amplitude changes sign with spin direction so that, although the interaction with a nucleus is still 'coherent', in the sense that the scattering amplitudes are summed, paired nucleons contribute zero scattering amplitude and only the residual unpaired nucleons contribute. Thus only nuclei with an odd number of protons and/or an odd number of neutrons can detect spin-dependent interactions.

The form of the spin dependence is typified by the cross-section for a hypothetical Majorana neutrino given by [2]

$$\sigma_{\nu_M} = \frac{2G_F^2}{\pi\hbar^4} \mu^2 I_s \quad (6.2)$$

where I_s is conventionally written in the form $I_s = C^2 \lambda^2 J(J+1)$. C is a factor related to the quark spin content of the nucleon:

$$C = \sum_q T_q^3 \Delta q, \quad (q = u, d, s)$$

where Δ_q is the fraction of the nucleon spin contributed by quark species q and $T_{u,d,s}^3 = \frac{1}{2}, -\frac{1}{2}, -\frac{1}{2}$, is the third component of isotopic spin for the respective quarks. In the single unpaired nucleon approximation,

$$\lambda^2 J(J+1) \equiv \frac{[J(J+1) + s(s+1) - \ell(\ell+1)]^2}{4J(J+1)},$$

but a more realistic value is obtained by assuming all nucleons of the same type as the unpaired nucleon contribute, with the net spin of these ‘odd-group’ nucleons estimated from the nuclear magnetic moment (μ_{mag}) [11]:

$$\lambda^2 J(J+1) = S_{\text{odd}}^2 \frac{J+1}{J},$$

where

$$S_{\text{odd}} = \frac{\mu_{\text{mag}} - g_N^\ell J}{g_N^s - g_N^\ell}$$

with $g_p^\ell = 1$, $g_n^\ell = 0$, $g_p^s = 5.586$, $g_n^s = -3.826$.

In addition to the spin-independent cross-section (6.1), a Dirac neutrino has a spin-dependent contribution one-quarter that given by (6.2) [2].

Interaction with the photino of supersymmetry theories [34] takes a similar form to (6.2):

$$\sigma_{\tilde{\gamma}} = \frac{1}{\pi} \mu^2 \lambda^2 J(J+1) \left[2 \sum_q \left(\frac{e Q_q}{m_{\tilde{q}} c} \right)^2 \Delta q \right]^2,$$

where $Q_{u,d,s} = \frac{2}{3}, -\frac{1}{3}, -\frac{1}{3}$ is the charge value for the respective quarks and $m_{\tilde{q}}$ is the mass of an exchanged squark³; in the case of squark mass degeneracy, this reduces to:

$$\sigma_{\tilde{\gamma}} = \frac{4}{\pi} \left(\frac{e}{m_{\tilde{q}} c} \right)^4 \mu^2 I_s \quad (6.3)$$

with C now given by $C = \sum_q Q_q^2 \Delta q$.

The ‘ e ’ in (6.3) arises from the substitution

$$\begin{aligned} e^2 &= 4\pi\alpha\hbar c \quad (\alpha = 1/137), \\ &= 4\sqrt{2} \frac{c}{\hbar} G_F M_W^2 \sin^2 \theta_W, \end{aligned}$$

which is correct apart from radiative correction terms of a few percent. Alternatively, (6.3) could be written:

$$\sigma_{\tilde{\gamma}} = \frac{2G_F^2}{\pi\hbar^4} \left(\frac{\sqrt{8} M_W \sin \theta_W}{m_{\tilde{q}}} \right)^4 \mu^2 I_s = \frac{2G_F^2}{\pi\hbar^4} \left(\frac{109 \text{ GeV} c^{-2}}{m_{\tilde{q}}} \right)^4 \mu^2 I_s.$$

In general the lightest (and hence most stable) supersymmetric particle (LSP) will be a mixture (a ‘neutralino’) of photino, Higgsino, Bino, and its cross-section for elastic scattering off nuclei will contain both spin-dependent and spin-independent terms [5,7,8,35]. In the approximation used above, the spin-independent term vanishes for pure gaugino or pure Higgsino states; the more general case is discussed in [6] and [9]—typically, the spin-independent term increases relative to the spin-dependant with increasing A , becoming dominant for $A \gtrsim 30$ [12].

³This assumes $m_{\tilde{q}} \gg m_{\tilde{\chi}}, M_T$, where $m_{\tilde{\chi}}$ is the neutralino mass. More generally, $m_{\tilde{q}}$ should be replaced throughout by $[(m_{\tilde{q}} + M_T)^2 - (m_{\tilde{\chi}} + M_T)^2]^{1/2}$ [35].

In the ‘full’ treatment of Engel et al. [11], I_s has contributions from both proton and neutron couplings:

$$I_s = [C_{Wp}\langle S_p \rangle + C_{Wn}\langle S_n \rangle]^2 \frac{J+1}{J},$$

where $\langle S_{p(n)} \rangle$ is the expectation value of the nuclear spin content due to the proton (neutron) group, calculated from the shell model.

6.3. Normalization of results

The need to normalize rate or cross-section when comparing results from different targets is seen by writing the generic low energy elastic cross-section as [2]

$$\sigma_0 \propto \left(\frac{g_D^2 g_N^2}{M_E^4} \right) \mu^2 \quad (6.4)$$

where g_D, g_N are the dimensionless coupling strengths to WIMP and nucleus, respectively, of a heavy exchanged particle of mass M_E . From (6.3) and (3.7), remembering that $\mu^2 = M_D M_T r / 4$,

$$\begin{aligned} \frac{R_0}{r} &\equiv 126 \left(\frac{\sigma_0}{1 \text{ pb}} \right) \left(\frac{1 \text{ GeV}c^{-2}}{\mu} \right)^2 \left(\frac{\rho_D}{0.4 \text{ GeV}c^{-2} \text{ cm}^{-3}} \right) \left(\frac{v_0}{230 \text{ km s}^{-1}} \right) \text{ tru} \\ &\propto \frac{g_D^2 g_N^2}{M_E^4}. \end{aligned} \quad (6.5)$$

Thus the quantities proportional to the fundamental interaction are either R_0/r or σ_0/μ^2 , and it is the limits on these⁴ (versus M_D) which should be shown, to remove the additional A -dependence in μ and r . Note that R_0 and σ_0 are defined as the values for zero momentum transfer, so the nuclear form factor has already been included in converting from observed rate to R_0 and σ_0 .

The coupling g_N to the target nucleus also contains an A -dependent coherent or spin factor, as discussed in Sections 6.1, 6.2, and where this is known theoretically it should also be included in the normalization:

(a) In the case of nuclear coherence it is sufficient to divide by A^2 or alternatively normalize to a specific nucleus, such as Ge. The plotted quantity is then

$$\left(\frac{R_0}{r} \text{ or } \frac{\sigma_0}{\mu^2} \right) \times \left[\left(\frac{1}{A_{\text{target}}} \right)^2 \text{ or } \left(\frac{A_{\text{Ge}}}{A_{\text{target}}} \right)^2 \right];$$

in normalizations for interactions such as that with a Dirac neutrino, A should be replaced by $N_1, \sim A - Z$ (to give the ‘WIMP-neutron’ cross-section σ_{Wn}).

(b) For the spin-dependent case, it is convenient to normalize from element A to the ‘WIMP-proton’ cross-section by the conversion

$$\sigma_{Wp}|_{\text{spin}} = \sigma_0 \times \frac{\mu_p^2}{\mu_T^2} \times \frac{[\lambda^2 J(J+1)]_p}{[\lambda^2 J(J+1)]_T} \times \left(\frac{C_{Wp}}{C_{WN}} \right)^2. \quad (6.6)$$

Values of the spin factor $\lambda^2 J(J+1)$ for some typical target elements are given in Table 3, for both the single particle and the odd group models.

Values of the WIMP-nucleon spin factor C_{WN}^2 depend on the values assumed for the quark spin fractions Δu , Δd , Δs ; and, while the nonrelativistic/naïve quark model (NQM) yields no strange quark content, European

⁴ Note that limits on R_0/r and σ_0/μ^2 are not ‘alternative presentations’—they are, from (6.5), identical curves, differing only in the labelling of the vertical axis.

Table 3
Values of $\lambda^2 J(J+1)$ for various isotopes

Isotope	J	$\lambda^2 J(J+1)$	
		single particle	odd group
^1H	1/2	0.75	0.75
^{19}F	1/2	0.75	0.647
^{23}Na	3/2	0.15	0.041
^{27}Al	5/2	0.35	0.087
^{43}Ca	7/2	0.321	0.152
^{73}Ge	9/2	0.306	0.065
^{93}Nb	9/2	0.306	0.162
^{127}I	5/2	0.35	0.007
^{129}Xe	1/2	0.75	0.124
^{131}Xe	3/2	0.15	0.055

Table 4
Values of WIMP-nucleon spin factors; $M_F = \sqrt{8} M_W \sin \theta_W \simeq 109 \text{ GeV}c^{-2}$

WN	C_{WN}^2			$\frac{\sigma_{WN} _{\text{spin}}}{\mu^2 I_s}$	$\frac{\sigma_{WN} _{\text{spin}}}{\sigma_{\nu MN}}$
	NQM	EMC [36]	EMC [4]		
$\tilde{\gamma}p$	0.14 ± 0.01	0.096 ± 0.009	0.06 ± 0.02	$\frac{4}{\pi} \left(\frac{e}{m_{\tilde{q}} c} \right)^4$	$\left(\frac{M_F}{m_{\tilde{q}}} \right)^4$
$\tilde{\gamma}n$	0.002 ± 0.001	0.012 ± 0.003	0.03 ± 0.01		
$\tilde{H}p$	0.40 ± 0.02	0.46 ± 0.04	0.55 ± 0.10	$\frac{8G_F^2}{\pi \hbar^4} \cos^2 2\beta$	$4 \cos^2 2\beta$
$\tilde{H}n$	0.40 ± 0.02	0.34 ± 0.03	0.26 ± 0.07		
$\tilde{B}p$	0.16 ± 0.01	0.10 ± 0.01	0.06 ± 0.02	$\frac{1}{\pi} \left(\frac{e}{m_{\tilde{q}} c} \right)^4 \frac{1}{\cos^2 \theta_W}$	$\left(\frac{M_F}{m_{\tilde{q}}} \right)^4 \frac{1}{4 \cos^2 \theta_W}$
$\tilde{B}n$	$(7 \pm 5) \times 10^{-4}$	0.010 ± 0.003	0.03 ± 0.01		
$\tilde{Z}p$	1.9 ± 0.1	0.9 ± 0.1	0.3 ± 0.2	$\frac{4}{\pi} \left(\frac{e}{m_{\tilde{q}} c} \right)^4 \tan^4 \theta_W$	$\left(\frac{M_F}{m_{\tilde{q}}} \right)^4 \tan^4 \theta_W$
$\tilde{Z}n$	0.21 ± 0.04	0.002 ± 0.006	0.1 ± 0.1		

Muon Collaboration (EMC) measurements indicate that strange quarks make a significant contribution to nucleon spin [4,10].

Ellis and Karliner [36] estimate $\Delta u = 0.83 \pm 0.03$, $\Delta d = -0.43 \pm 0.03$, $\Delta s = -0.10 \pm 0.03$ for EMC; comparable estimates for NQM are $\Delta u = 0.93 \pm 0.02$, $\Delta d = -0.33 \pm 0.02$ (and $\Delta s \equiv 0$). Both these estimates are for protons; for neutrons, the numerical values of $\Delta u, \Delta d$ are exchanged. C_{WN}^2 resulting from these Δq are tabulated in Table 4 for various WIMP interactions; values for a Majorana neutrino are the same as those for a Higgsino.

A number of experimental papers use C_{WN}^2 values from the earlier [4], based on $\Delta u = 0.74 \pm 0.08$, $\Delta d = -0.51 \pm 0.08$, $\Delta s = -0.23 \pm 0.08$; since the photino values in particular are quite different, these earlier values are also shown in Table 4. From the experimentalist's point of view, the important thing is the relative sensitivity of odd- N (Ge, Xe, Ca) and odd- Z (Na, I, F) targets—i.e. the ratio σ_{Wp}/σ_{Wn} ; the ‘old’ values [4] conveniently gave ~ 2 for this ratio whatever the neutralino, whereas the revised values [36] yield a ratio which is close to unity for \tilde{H} but $\gtrsim 10$ otherwise. Within the estimated errors, similar conclusions result from the Δq values derived in [37] for both the ‘standard’ treatment and a ‘valence’ treatment in which $\Delta s \equiv 0$ is possible.

The final column of Table 4 compares cross-sections with that for a Majorana neutrino, from (6.1); $M_F = \sqrt{8} M_W \sin \theta_W \simeq 109 \text{ GeV}c^{-2}$.

6.4. Combining results

Following application of the various factors discussed above, experimental results are typically in the form of estimates of rate (or cross-section) and its standard deviation, derived for each of a number of energy bins. In the absence of systematic errors and of any correlation effects such results, and comparable results from other detectors, can be combined using the standard expressions:

$$\widehat{R}_0 = \frac{1}{w} \sum_{i=1}^N w_i R_{0i}, \quad \widehat{S} = 1/\sqrt{w}, \quad (6.7)$$

where $w_i = 1/S_i^2$, $w = \sum_{i=1}^N w_i$, for N independent rate estimates R_{0i} with corresponding estimated standard deviation S_i .

Appendix A. Derivation of results in Sections 2-3

(A slightly more detailed version of this appendix appears in the preprint RAL-TR-95-024.)

The results quoted in Section 2 can be derived as follows: for $v_{\text{esc}} = \infty$ we have, for a 'stationary' Earth ($v_E = 0$),

$$k_0 = \int_0^{2\pi} d\phi \int_{-1}^{+1} d(\cos \theta) \int_0^{\infty} e^{-v^2/v_0^2} v^2 dv = 4\pi \int_0^{\infty} e^{-v^2/v_0^2} v^2 dv = (\pi v_0^2)^{3/2}.$$

Since particle density is clearly independent of v_E , k must also be independent of v_E ; this can be used as a check on formulae for a 'moving' Earth, for which $(v + v_E)^2 = v^2 + v_E^2 + 2vv_E \cos \theta$:

$$\begin{aligned} k &= \int_0^{2\pi} d\phi \int_{-1}^{+1} d(\cos \theta) \int_0^{\infty} e^{-(v + v_E)^2/v_0^2} v^2 dv \\ &= 2\pi \int_0^{\infty} e^{-(v^2 + v_E^2)/v_0^2} v^2 \int_{-1}^{+1} e^{-2vv_E \cos \theta/v_0^2} d(\cos \theta) dv \\ &= \frac{\pi v_0^2}{v_E} \int_0^{\infty} v \left[e^{-(v - v_E)^2/v_0^2} - e^{-(v + v_E)^2/v_0^2} \right] dv \\ &= \frac{\pi v_0^2}{v_E} \left[\int_{-v_E}^{\infty} (x + v_E) e^{-x^2/v_0^2} dx - \int_{v_E}^{\infty} (x - v_E) e^{-x^2/v_0^2} dx \right] \\ &= \frac{\pi v_0^2}{v_E} \left[\int_{-v_E}^{v_E} x e^{-x^2/v_0^2} dx + 2v_E \int_0^{\infty} e^{-x^2/v_0^2} dx \right] \\ &= \frac{\pi v_0^2}{v_E} \left[0 + 2v_E \frac{\pi^{1/2}}{2} v_0 \right] \equiv k_0. \end{aligned}$$

For $v_{\text{esc}} \neq \infty, v_E = 0$,

$$k_1 = \int_0^{2\pi} d\phi \int_{-1}^{+1} d(\cos \theta) \int_0^{v_{\text{esc}}} e^{-v^2/v_0^2} v^2 dv = 4\pi \int_0^{v_{\text{esc}}} e^{-v^2/v_0^2} v^2 dv;$$

then, since

$$\int_0^{v_{\text{esc}}} e^{-v^2/v_0^2} dv = \frac{2}{v_0^2} \left[\int_0^{v_{\text{esc}}} e^{-v^2/v_0^2} v^2 dv + v_{\text{esc}} e^{-v_{\text{esc}}^2/v_0^2} \right],$$

$$k_1 = 2\pi v_0^2 \left[\int_0^{v_{\text{esc}}} e^{-v^2/v_0^2} dv - v_{\text{esc}} e^{-v_{\text{esc}}^2/v_0^2} \right] = k_0 \left[\text{erf} \left(\frac{v_{\text{esc}}}{v_0} \right) - \frac{2}{\pi^{1/2}} \frac{v_{\text{esc}}}{v_0} e^{-v_{\text{esc}}^2/v_0^2} \right].$$

The differential and total rates (Section 3) require evaluation of similar integrals, differing only by factors v^2/v_0^2 and $E_0 r$ in the integrand, and in the lower limit of integration (v_{min} for the former, 0 for the latter). Thus

$$\begin{aligned} \frac{dR(0, v_{\text{esc}})}{dE_R} &= \frac{R_0}{E_0 r} \frac{k_0}{k_1} \frac{1}{2\pi v_0^2} \int_0^{2\pi} d\phi \int_{-1}^{+1} d(\cos \theta) \int_{v_{\text{min}}}^{v_{\text{esc}}} e^{-v^2/v_0^2} v dv \\ &= \frac{R_0}{E_0 r} \frac{k_0}{k_1} \frac{2}{v_0^2} \int_{v_{\text{min}}}^{v_{\text{esc}}} e^{-v^2/v_0^2} v dv \\ &= \frac{R_0}{E_0 r} \frac{k_0}{k_1} \int_{E_R/E_0 r}^{v_{\text{esc}}/v_0^2} e^{-x} dx \\ &= \frac{R_0}{E_0 r} \frac{k_0}{k_1} \left(e^{-E_R/E_0 r} - e^{-v_{\text{esc}}^2/v_0^2} \right); \end{aligned}$$

while

$$\begin{aligned} \frac{R(0, v_{\text{esc}})}{R_0} &= \frac{k_0}{k_1} \int_0^{v_{\text{esc}}/v_0^2} x e^{-x} dx \\ &= \frac{k_0}{k_1} \left[1 - \left(1 + \frac{v_{\text{esc}}^2}{v_0^2} \right) e^{-v_{\text{esc}}^2/v_0^2} \right]. \end{aligned}$$

For $v_E \neq 0$, evaluations are similar to that of k above:

$$\begin{aligned} \frac{dR}{dE_R} &= \frac{R_0}{E_0 r} \frac{k_0}{k} \frac{1}{2v_E} \left[\int_{v_{\text{min}}}^{v_{\text{esc}} + v_E} e^{-(v - v_E)^2/v_0^2} dv - \int_{v_{\text{min}}}^{v_{\text{esc}} - v_E} e^{-(v + v_E)^2/v_0^2} dv - e^{-v_{\text{esc}}^2/v_0^2} \int_{v_{\text{esc}} - v_E}^{v_{\text{esc}} + v_E} dv \right] \\ &= \frac{R_0}{E_0 r} \frac{k_0}{k} \left\{ \frac{1}{2v_E} \left[\int_{v_{\text{min}} - v_E}^{v_{\text{esc}}} e^{-w^2/v_0^2} dw - \int_{v_{\text{min}} + v_E}^{v_{\text{esc}}} e^{-w^2/v_0^2} dw \right] - e^{-v_{\text{esc}}^2/v_0^2} \right\} \\ &= \frac{R_0}{E_0 r} \frac{k_0}{k} \left\{ \frac{\pi^{1/2}}{4} \frac{v_0}{v_E} \left[\text{erf} \left(\frac{v_{\text{min}} + v_E}{v_0} \right) - \text{erf} \left(\frac{v_{\text{min}} - v_E}{v_0} \right) \right] - e^{-v_{\text{esc}}^2/v_0^2} \right\} \end{aligned}$$

which leads to (3.12) or (3.13) according to the value of v_{esc} .

Similarly,

$$\begin{aligned} \frac{R}{R_0} &= \frac{k_0}{k} \frac{1}{2v_0^2 v_E} \left[\int_0^{v_{\text{esc}} + v_E} v^2 e^{-(v - v_E)^2/v_0^2} dv - \int_0^{v_{\text{esc}} - v_E} v^2 e^{-(v + v_E)^2/v_0^2} dv - e^{-v_{\text{esc}}^2/v_0^2} \int_{v_{\text{esc}} - v_E}^{v_{\text{esc}} + v_E} v^2 dv \right] \\ &= \frac{1}{2} \frac{k_0}{k} \left[\pi^{1/2} \left(\frac{v_E}{v_0} + \frac{1}{2} \frac{v_0}{v_E} \right) \operatorname{erf} \left(\frac{v_E}{v_0} \right) + e^{-v_E^2/v_0^2} - 2 \left(\frac{v_{\text{esc}}^2}{v_0^2} + \frac{1}{3} \frac{v_E^2}{v_0^2} + 1 \right) e^{-v_{\text{esc}}^2/v_0^2} \right], \end{aligned}$$

giving (3.4) and (3.5).

Finally, integration of the angular distribution (3.16) is achieved by making the substitution $w = (v_{\text{min}} - v_E \cos \psi)/v_0$:

$$\begin{aligned} \frac{dR(v_E, \infty)}{dE_R} &= \frac{1}{2} \frac{R_0}{E_0 r} \int_{-1}^{+1} e^{-(v_E \cos \psi - v_{\text{min}})^2/v_0^2} d(\cos \psi) \\ &= \frac{1}{2} \frac{R_0}{E_0 r} \frac{v_0}{v_E} \int_{(v_{\text{min}} - v_E)/v_0}^{(v_{\text{min}} + v_E)/v_0} e^{-x^2} dx \\ &= \frac{R_0}{E_0 r} \frac{\pi^{1/2}}{4} \frac{v_0}{v_E} \left[\operatorname{erf} \left(\frac{v_{\text{min}} + v_E}{v_0} \right) - \operatorname{erf} \left(\frac{v_{\text{min}} - v_E}{v_0} \right) \right]. \end{aligned}$$

Appendix B. Velocities

Druckier et al. [38] argue that $v_0 = u_r$ (the galactic rotation velocity) for a galaxy with a flat rotation curve. Reported values for u_r are: $243 \pm 20 \text{ km s}^{-1}$ [39]; $222 \pm 20 \text{ km s}^{-1}$ [40]; and $228 \pm 19 \text{ km s}^{-1}$ [41]. We use $v_0 = u_r = 230 \text{ km s}^{-1}$.

According to Druckier et al. [38], $580 \text{ km s}^{-1} < v_{\text{esc}} \leq 625 \text{ km s}^{-1}$; we take $v_{\text{esc}} = 600 \text{ km s}^{-1}$. However, Cudworth [42] finds an appreciably smaller lower limit: $v_{\text{esc}} > 475 \text{ km s}^{-1}$.

The target velocity relative to the dark matter halo, v_E , is the sum of three motions:

$$v_E = u_r + u_s + u_E;$$

in galactic co-ordinates, these are:

- the galactic rotation,

$$u_r = (0, 230, 0) \text{ km s}^{-1};$$

- the Sun's 'proper motion', i.e. its mean motion relative to nearby stars⁵ [43],

$$u_s = (9, 12, 7) \text{ km s}^{-1};$$

- and the Earth's orbital velocity relative to the Sun:

$$u_{E_x} = u_E(\lambda) \cos \beta_x \sin(\lambda - \lambda_x),$$

$$u_{E_y} = u_E(\lambda) \cos \beta_y \sin(\lambda - \lambda_y),$$

$$u_{E_z} = u_E(\lambda) \cos \beta_z \sin(\lambda - \lambda_z)$$

⁵ Standard deviations appear to be $\sim 0.3 \text{ km s}^{-1}$.

Table C.1

Seasonal variation of velocity, rates, and parameters c_1, c_2

Period	year	Jan	Feb	Mar	Apr	May	Jun	Jul	Aug	Sep	Oct	Nov	Dec
$v_E(\text{km s}^{-1})$	244.0	233.4	240.0	247.4	253.7	257.2	257.4	254.3	248.5	241.4	234.6	230.0	229.5
$\frac{R(v_E, \infty)}{R_0}$	1.339	1.313	1.329	1.347	1.364	1.373	1.373	1.365	1.350	1.332	1.315	1.304	1.303
$\frac{R(v_E, v_{\text{esc}})}{R_0}$	1.334	1.308	1.324	1.343	1.359	1.368	1.369	1.361	1.346	1.328	1.311	1.300	1.299
c_1	0.751	0.766	0.757	0.747	0.738	0.734	0.734	0.738	0.745	0.755	0.764	0.770	0.771
c_2	0.561	0.583	0.569	0.554	0.542	0.535	0.534	0.540	0.552	0.567	0.581	0.590	0.592

where λ is the ecliptic longitude, ~ 0 at the vernal equinox and increasing by $\sim 1^\circ$ per day;

$$\begin{aligned} \beta_x &= -5^\circ.5303, & \beta_y &= 59^\circ.575, & \beta_z &= 29^\circ.812, \\ \lambda_x &= 266^\circ.141, & \lambda_y &= -13^\circ.3485, & \lambda_z &= 179^\circ.3212, \end{aligned}$$

are the ecliptic latitudes (β) and longitudes (λ) of the x, y, z axes in galactic coordinates; and

$$u_E(\lambda) = \langle u_E \rangle [1 - e \sin(\lambda - \lambda_0)],$$

where $\langle u_E \rangle = 29.79 \text{ km s}^{-1}$ is the Earth's mean orbital velocity, $e = 0.016722$ is the ellipticity of the Earth's orbit, and $\lambda_0 = 13^\circ \pm 1^\circ$ is the longitude of the orbit's minor axis.

λ is estimated from the formula [44]

$$\lambda = L + 1^\circ.915 \sin g + 0^\circ.020 \sin 2g,$$

where $L = 280^\circ.460 + 0^\circ.9856474 n$, and $g = 357^\circ.528 + 0^\circ.9856003 n$, (both modulo 360°), where n is the (fractional) day number relative to noon (UT) on 31 December 1999 (referred to in [44] as "J2000.0").

Errors in λ from this formula in the 4-year period 1987-90 reached a minimum of $-45''$ in June 1987 and a maximum of $3''$ in April 1989 (i.e. a time error between -18 and $+1$ minutes), with a mean of $-18'' \pm 11''$ ($\sim 7 \pm 4$ minutes).

Appendix C. Annual modulation of coefficients c_1, c_2

Rate dependence on v_E is given in Table C.1, as mean annual and monthly values. Maxima occur on June 1st or 2nd:

$$(v_E)_{\text{max}} = 258 \text{ km s}^{-1}, \quad [R(v_E, \infty)/R_0]_{\text{max}} = 1.374, \quad [R(v_E, v_{\text{esc}})/R_0]_{\text{max}} = 1.370;$$

and minima on December 3rd or 4th:

$$(v_E)_{\text{min}} = 229 \text{ km s}^{-1}, \quad [R(v_E, \infty)/R_0]_{\text{min}} = 1.302, \quad [R(v_E, v_{\text{esc}})/R_0]_{\text{min}} = 1.298.$$

Values determined by a one-parameter least squares fit to (3.14) over the energy range⁶ $0 \leq E_R \leq 20 \times E_{0r}$ are also given in Table C.1. The dependence of c_1 on v_E is strongly linear, with $c_1 = 1.077 - 0.001336 \times v_E$ accurate to better than 0.1% over the range of Table C.1.

In practical situations, noise and background result in a minimum effective detectable energy. Consequently, the energy range used in determining c_1, c_2 should be the *usable* energy range; the dependence of E_{0r} on

⁶ For $v_{\text{esc}} = 600 \text{ km s}^{-1}$, $E_R/E_{0r} < 14$.

Table C.2

Energy threshold dependence of c_1 coefficients a, b

x_1	$\leq 10^{-3}$	0.002	0.005	0.01	0.02	0.05	0.1	0.2	0.5	1.0	2.0	5.0	10.0
a	1.077	1.077	1.077	1.077	1.076	1.075	1.073	1.069	1.053	1.015	1.064	1.055	1.005
$10^3 \times b$ (km^{-1}s)	1.333	1.332	1.331	1.329	1.325	1.312	1.292	1.251	1.125	0.965	1.220	0.952	0.480

M_D, M_T and the dependence of detection efficiency on M_T then mean that c_1, c_2 vary with M_D, M_T . Expressed in terms of the dimensionless variable $x_1 = E_R/E_0 r$,

$$c_1(x_1, x_2, v_E) = a(x_1, x_2) - b(x_1, x_2) \times v_E,$$

for the energy range given by $x_1 \leq x \leq x_2$, with c_2 determined from:

$$\frac{c_1}{c_2} = \frac{R(v_E, \infty)}{R_0}.$$

Dependence on x_2 is slight; values of a, b for various x_1 are given in Table C.2 (with $x_2 \sim 14$, the limiting value when $v_{\text{esc}} = 600 \text{ km s}^{-1}$).

References

- [1] M.W. Goodman and E. Witten, Phys. Rev. D 31 (1985) 3059.
- [2] J.R. Primack, D. Seckel and B. Sadoulet, Ann. Rev. Nucl. Part. Sci. 38 (1988) 751.
- [3] P.F. Smith and J.D. Lewin, Physics Reports 187 (1990) 203.
- [4] J. Ellis and R.A. Flores, Nucl. Phys. B 307 (1988) 883.
- [5] K. Griest, Phys. Rev. Lett. 62 (1988) 666; Phys. Rev. D 38 (1988) 2357.
- [6] M. Srednicki and R. Watkins, Phys. Lett. B 225 (1989) 140.
- [7] R. Barbieri, M. Frigeni and G.F. Giudice, Nucl. Phys. B 313 (1989) 725.
- [8] G.B. Gelmini, P. Gondolo and E. Roulet, Nucl. Phys. B 351 (1991) 623.
- [9] M. Drees and M.K. Nojiri, Phys. Rev. D 48 (1993) 3483.
- [10] J. Ellis and R.A. Flores, Phys. Lett. B 263 (1991) 259.
- [11] J. Engel, S. Pittel and P. Vogel, Int. J. Mod. Phys. E 1 (1992) 1.
- [12] G. Jungman, M. Kamionkowski and K. Griest, Physics Reports 267 (1996) 195.
- [13] E.I. Gates, G. Gyuk and M.S. Turner, Astrophys. J. 449 (1995) L123.
- [14] D.N. Spergel, Phys. Rev. D 37 (1988) 1353.
- [15] J. Engel, Phys. Lett. B 264 (1991) 114.
- [16] J. Engel, personal communication.
- [17] E.g., R. Hofstadter, Rev. Mod. Phys. 28 (1956) 214.
- [18] G. Fricke et al., Atomic Data and Nuclear Data Tables 60 (1995) 177.
- [19] A. Bottino and J. Engel, personal communications.
- [20] E.g., Y.N. Kim, S. Wald and A. Ray, Radial Shape of Nuclei (invited papers, 2nd Nucl. Phys. Divisional Conf. of the European Phys. Soc., Cracow, eds. A. Budzanowski and A. Kapuścik) (1976) pp. 33-52.
- [21] R.H. Helm, Phys. Rev. 104 (1956) 1466.
- [22] R.C. Barrett and D.F. Jackson, Nuclear Sizes and Structure (Oxford, 1977).
- [23] G. Eder, Nuclear Forces (MIT Press, 1968), Chapter 7.
- [24] A. Gould, Ap. J. 321 (1987) 571.
- [25] J. Lindhard et al., K. Dan. Vidensk. Selsk., Mat.-Fys. Medd. 33 (1963) No. 10; 36 (1968) No. 10.
- [26] N.J.C. Spooner et al., Phys. Lett. B 321 (1994) 156.
- [27] G.J. Davies et al., Phys. Lett. B 322 (1994) 159.
- [28] E.g. J.D. Lewin and P.F. Smith, Phys. Rev. D 32 (1985) 1177.
- [29] D.J. Ficenec et al., Phys. Rev. D 36 (1987) 311.

- [30] E.g. G.F. Knoll, *Radiation Detection and Measurement* (Wiley, 1979).
- [31] N.J.T. Smith, C.H. Lally and G.J. Davies, *Nucl. Phys. B Proc. Suppl.* 48 (1996) 67.
- [32] J.J. Quenby et al., *Phys. Lett. B* 351 (1995) 70.
- [33] P.F. Smith et al., *Phys. Lett. B* 379 (1996) 299.
- [34] H.E. Haber and G.L. Kane, *Physics Reports* 117 (1985) 75.
- [35] M. Kamionkowski, *Phys. Rev. D* 44 (1991) 3021.
- [36] J. Ellis and M. Karliner, *Phys. Lett. B* 341 (1995) 397.
- [37] M. Glück, E. Reya and W. Vogelsang, *Phys. Lett. B* 359 (1995) 201.
- [38] A.K. Drukier, K. Freese and D.N. Spergel, *Phys. Rev. D* 33 (1986) 3495.
- [39] G.R. Knapp, S.D. Tremaine and J.E. Gunn, *Astron. J.* 83 (1978) 1585.
- [40] F.J. Kerr and D. Lynden-Bell, *MNRAS* 221 (1986) 1023.
- [41] J.A.R. Caldwell and J.M. Coulson, *Astron. J.* 93 (1987) 1090.
- [42] A.J. Cudworth, *Astron. J.* 99 (1990) 590.
- [43] D. Mihalas and J. Binney, *Galactic Astronomy* (Freeman, San Francisco, 1981).
- [44] The Astronomical Almanac, p. C24 (HMSO, yearly).
- [45] I.S. Gradshteyn and I.M. Ryzhik, *Table of Integrals, Series, and Products, Corrected and Enlarged Edition* (Academic Press, 1980).